Original Article

3D printed PLGA/MgO/PDA composite scaffold by low-temperature deposition manufacturing for bone tissue engineering applications

Liang Tan [a, b], Zhuofeng Ye [c], Weida Zhuang [a, b], Beini Mao [a], Hetong Li [a], Xiuwang Li [a, b], Jiachang Wu [a, b], Hongxun Sang [a, b, *]

[a] Department of Orthopedics, Shenzhen Hospital, Southern Medical University, 1333 Xinhu Road, Shenzhen, Guangdong, 518000, PR China
[b] The Third School of Clinical Medicine, Southern Medical University, Guangzhou, China
[c] Department of Orthopedics, Jiangmen Central Hospital, Jiangmen, China

ARTICLE INFO

ABSTRACT

Introduction: Bones are easily damaged. Biomimetic scaffolds are involved in tissue engineering. This study explored polydopamine (PDA)-coated poly lactic-co-glycolic acid (PLGA)-magnesium oxide (MgO) scaffold properties and its effects on bone marrow mesenchymal stem cells (BMSCs) osteogenic differentiation.
Methods: PLGA/MgO scaffolds were prepared by low-temperature 3D printing technology and PDA coatings were prepared by immersion method. Scaffold structure was observed by scanning electron microscopy with an energy dispersive spectrometer (SEM-EDS), fourier transform infrared spectrometer (FTIR). Scaffold hydrophilicity, compressive/elastic modulus, and degradation rates were analyzed by water contact angle measurement, mechanical tests, and simulated-body fluid immersion. Rat BMSCs were cultured in scaffold extract. Cell activity on days 1, 3, and 7 was detected by MTT. Cells were induced by osteogenic differentiation, followed by evaluation of alkaline phosphatase (ALP) activity on days 3, 7, and 14 of induction and Osteocalcin, Osteocalcin, and Collagen I expressions.
Results: The prepared PLGA/MgO scaffolds had dense microparticles. With the increase of MgO contents, the hydrophilicity was enhanced, scaffold degradation rate was accelerated, magnesium ion release rate and scaffold extract pH value were increased, and cytotoxicity was less when magnesium mass ratio was less than 10%. Compared with other scaffolds, compressive and elastic modulus of PLGA/MgO (10%) scaffolds were increased; BMSCs incubated with PLGA/MgO (10%) scaffold extract had higher ALP activity and Osteocalcin, Osteopontin, and Collagen I expressions. PDA coating was prepared in PLGA/MgO (10%) scaffolds and the mechanical properties were not affected. PLGA/MgO (10%)/PDA scaffolds had better hydrophilicity and biocompatibility and promoted BMSC osteogenic differentiation.
Conclusion: Low-temperature 3D printing PLGA/MgO (10%)/PDA scaffolds had good hydrophilicity and biocompatibility, and were conducive to BMSC osteogenic differentiation.
© 2023, The Japanese Society for Regenerative Medicine. Production and hosting by Elsevier B.V. This is an open access article under the CC BY-NC-ND license (http://creativecommons.org/licenses/by-nc-nd/4.0/).

1. Introduction

Bones are prone to be damaged in the human body due to a variety of causes including diseases, infections, and fractures, which have a remarkable capacity to heal and repair themselves after illness and trauma [1]. However, large defects can never be reinstated completely as the sizes are larger than the limit up to which the bones can heal and repair, and as a result, medical treatment is required to align, support, and stabilize the damaged bone to restore the function [2]. Tissue engineering is a promising treatment consisting of a biocompatible scaffold, appropriate growth factors, and stem cells [3]for human bone defects, which remain a major threat to human health and cannot be treated completely using current methods [4]. Biomimetic scaffolds can provide a tissue-specific environment to cells and are particularly promising for tissue engineering [5]. A scaffold with high

properties underpins the success of the strategy of bone tissue engineering, and the main direction in this field is to produce bone tissue engineering scaffolds with desirable structural, shape, biological, chemical, and physical features for complex regenerating bone tissues and enhanced biological properties [6]. Three-dimensional (3D) printing technology allows functional structure reproducible and automated manufacturing for tissue engineering with customized compositions and geometries through depositing materials layer-by-layer [7]. 3D printing technology that mimics the healing processes of physiological bone can achieve promising repair outcomes [8]. Among various 3D printing technologies, low-temperature biological 3D printing is the process of making porous scaffolds from composite materials using printing equipment based on the model path. After vacuum freeze-drying and solvent sublimation, a large number of micropores are formed. Due to the formation in a low-temperature environment, not only can the pore size, porosity, and specific surface area of the scaffolds be regulated, but also it is beneficial to maintain the biological activity of raw materials and achieve complementary advantages of the composite materials [9], which is considered the most suitable method for bone defect repair in the future [10,11]. Low-temperature 3D printing technology requires exploring corresponding printing parameters for different biological materials. Especially, determining the printing parameters of multiple composite materials is more difficult. Therefore, selecting proper and reasonable scaffold materials is particularly principal for bone tissue repair.

Poly lactic-co-glycolic acid (PLGA) is a synthetic lipophilic polymer material, which is widely used in the research of tissue engineering bone repair materials [12]. The advantages of PLGA are good biocompatibility, non-toxicity, easy processing, and controllable biodegradation rate and the disadvantages are poor mechanical properties, hydrophobicity, and the degradation products are acidic, which may cause a local inflammatory reaction [13]. Magnesium oxide (MgO) has excellent tensile strength and elastic modulus, and the composite of MgO and polyester possesses high mechanical strength and fracture toughness and meets the mechanical requirements of bone repair materials [14]. Magnesium scaffolds have good biocompatibility and can promote bone activity [15]. In the degradation process, it can neutralize the acidic substances produced by the degradation of polyester materials, improve the pH value, and then reduce the local inflammation, and the generated magnesium ions can effectively activate bone cells [16]. The PLGA/MgO scaffold facilitates osteogenesis by regulating the continuous release of Mg^{2+} [17—19]. However, although Mg^{2+} are biologically active and have been shown to facilitate regeneration of bone tissues, the functions of Mg^{2+} strongly depend on concentration, and high Mg^{2+} levels may impair osteoblast activity and lead to bone diseases [20,21]. Although this ability may have a significant impact on bone regeneration, there is currently no mature bone tissue engineering scaffold that can accurately modulate the release of Mg^{2+}. In addition, MgO is an alkaline inorganic material that can disrupt the acid-base balance in the organism, leading to tissue damage and inflammatory reactions, thereby affecting the repair effect [22]. Therefore, reducing the corrosion rate of magnesium alloy in PLGA/MgO scaffolds and controlling the concentration of Mg^{2+} are essential to ensure bone regeneration and functional reconstruction.

Polydopamine (PDA) is formed by dopamine self-polymerization under alkaline conditions and has good adhesion and biocompatibility, and can better promote cell adhesion and proliferation [23]. PDA has been widely used for surface modification of biological materials [24—26]. Also, PDA has a unique chemical structure and good biocompatibility that can be tightly bound to almost all types of surfaces to improve the stability of multi-component materials [27]. Moreover, PDA can reduce the

corrosion rate of magnesium alloys and regulate the release of magnesium ions [28]. Therefore, the preparation of novel PLGA/MgO/PDA scaffolds with suitable porous structure, suitable biodegradability and non-irritation using low-temperature 3D printing technology has great attraction for the repair of bone defects. In this study, the PLGA/MgO/PDA composite scaffolds were prepared by low-temperature 3D printing technology combined with dissolution and immersion method to explore the properties of scaffolds and their effects on osteogenic differentiation of bone marrow mesenchymal stem cells (BMSCs).

2. Materials and methods

2.1. Ethics statement

All procedures were authorized by the academic ethics committee of Shenzhen Hospital, Southern Medical University. All the laboratory procedures were used to reduce the pain of the rats.

2.2. Scaffolds fabrication

PLGA (75:25) (Shandong Institute of Medical Instruments, Jinan, Shandong, China) was dissolved in 1,4-dioxane (MACLIN Reagent, Shanghai, China) and supplemented with MgO powders (XFNANO, Nanjing, Jiangsu, China) with the particle size of around 20 nm to form a uniform solution at a ratio of 19/1 (w/w of PLGA/MgO, P5MgO), 18/2 (w/w of PLGA/MgO, P10MgO), 17/3 (w/w of PLGA/MgO, P15MgO) and PLGA. Subsequently, the paste was stirred vigorously overnight using a magnetic stirrer (Thermo Fisher Scientific Inc., Waltham, MA, USA). The paste was spurted out at a distance of 1.2 mm and the thickness of 200 μm layer-by-layer using a low-temperature deposition 3D printing machine (Bio-Architect®-WS, Hangzhou Regenovo Biotechnology, Hangzhou, Zhejiang, China). The diameter of the nozzle was 410 μm, and the migration velocity was 28 mm/s. The paste was extruded out of the nozzle through the propeller, with the working table system making a synthetic movement along the x-y-axes and the nozzle moving along the z-axis. The thickness of the slice was set to 200 μm. An XXYY laminated design (each slice was repeated twice) was employed to elevate the porosity (Supplementary Fig. 1). The ambient temperature was set at −25 °C. After that, the scaffolds were lyophilized in a freeze dryer (Bo Yi Kang FD-1- 50, China) for 24 h under 20—40 Pa pressure of a vacuum and sealed in plastic bags. The PDA coating was prepared. The scaffolds to be coated were soaked in PDA solution (2 mg/mL, in 10 mM Tris-HCl, pH 8.5), shaken on a shaker at room temperature for 12 h, and then rinsed with deionized water 3 times.

2.3. Scanning electron microscope observation with energy dispersive spectrometer (SEM-EDS)

The scaffolds were washed, fixed, dehydrated with gradient ethanol, and dried at room temperature. After gold sputtering, the microstructure and pore size and the elemental compositions of the scaffolds were observed using an SEM-EDS (S-4800, Hitachi, Tokyo, Japan). Three samples were set up for each scaffold to measure and take the average value.

2.4. Fourier transform infrared (FTIR) analysis

The attenuated total reflection (ATR) mode of the Avatar 370 infrared spectrometer (FT-IR, Nicolette, USA) was employed to analyze the functional group structure of the scaffolds. The scanning range was 4000—400 cm^{-1} and the resolution was 1 cm^{-1}. The

component or coating of the scaffolds was scraped off, mixed with potassium bromide (KBr), and pressed evenly for FTIR analysis.

2.5. Hydrophilic nature detection

The scaffold samples of each group were dripped with deionized water and the water contact angle of the scaffolds was tested using a water contact angle measuring instrument (SCI3000F, Huanqiu-hengda Technology, Beijing, China). Each sample was repeatedly tested 3 times.

2.6. Measurement of scaffold porosity using the ethanol replacement method

The scaffolds with the original weight of Ws were placed into the weighing bottle pre-filled with ethanol and weighed as W1. After the bottle was vacuumized and the micropores of the scaffolds were filled with ethanol, the scaffolds were taken out, and the weighing bottle was weighed as W2. The porosity of the scaffolds = $100\% \times (W1-W2-Ws)$/ethanol density/external volume of the scaffolds.

2.7. Mechanical property test

The size of the scaffolds was designed as $10 \times 10 \times 10$ mm. The compressive strength and elastic modulus of the scaffolds were tested using a universal mechanical testing machine (Z050, Zwick/Roell, Ulm, Germany) at room temperature under dry conditions. The movement speed of the pressure head was 1 mm/min. Each scaffold was repeatedly tested 6 times to take the average value. The measurement was following the standard of ISO 844:2021.

2.8. Scaffold degradation test

The size of scaffolds was prepared as 10 mm $\times$ 10 mm $\times$ 10 mm. The scaffolds were soaked in the solution according to the ratio (1 g: 10 mL) of scaffold weight to phosphate-buffered saline (PBS) volume and the initial pH value (7.4) of the solution at 37 °C. Before soaking, the scaffolds were weighed as W0. After 1 week of soaking, the scaffolds were taken out, the scaffolds were lyophilized in a freeze dryer for 24 h under 20–40 Pa pressure of a vacuum, and weighed as Wt. The degradation rate was WL = (W0 - Wt)/W0 $\times$ 100%. The scaffolds were soaked for 5 weeks. On the 1st, 3rd, 7th, 14th, 21st, 28th, and 35th d of the soaking, the concentration of Mg ions in the solution was determined using an inductively coupled plasma mass spectrometer (Agilent 7700X ICP-MS, CA, USA), and the release curve was drawn. The pH value changes of the soaking solution collected at each time point were detected using a pH meter (Shengaohua, Shanghai, China). Each time after the liquid was collected, and the solution was added with the same volume of PBS to keep the volume of the original solution unchanged. Four samples of each kind of scaffold were tested to take the average value.

2.9. Isolation and culture of BMSCs

Healthy adult Sprague-Dawley rats were euthanized after anesthesia and soaked with 75% ethanol for 10 min. The long bones of the limbs were collected, and the metaphysis was removed. Then, the bone marrow cavity was exposed and rinsed with Dulbecco's modified Eagle's medium (DMEM) low sugar-medium (Thermo Fisher Scientific Inc.). After that, the flushing fluid was collected and repeatedly dispersed with a syringe, and the single-cell suspension was obtained and cultured in a 25 cm^2 culture bottle in an incubator containing 5% CO$_2$ at 37 °C. The medium was refreshed every 2–3 d. The primary culture was terminated when the confluence of the adherent cells reached 80% and the cells were then subcultured at the ratio of 1:3. The cell growth was daily observed using an inverted phase-contrast microscope (CKX53, Olympus, Tokyo, Japan).

2.10. Identification of BMSCs

The P3 generation cells with good growth conditions were collected, detached with 0.25% trypsin, centrifuged at 4 °C at 300 g for 3 min, and washed with PBS 3 times. Then, the cell concentration was adjusted to 1×10^5 cells/mL. Each of the specific tubes for flow cytometry was added with 100 μL cell suspension, CD29 PE-Cyanine7 antibody (25-0291-82, eBioscience™, San Diego, CA, USA), CD34 Alexa Fluor® 488 antibody (NBP2-34713AF488, Novus Biologicals, Littleton, CO, USA), CD44 PE antibody (12-0444-82, eBioscience™), CD45 FITC antibody (11-0461-82, eBioscience™) and the negative control group was set for each tube (IgG was used as the homotypic negative control). The samples were incubated for 15 min in the dark. Each sample was added with 2 mL flow buffer, washed 3 times to remove the unbound antibody, and centrifuged at 300 g for 5 min, and the supernatant was removed. The cells were resuspended with 500 μL flow buffer and detected using a flow cytometer (MoFloAstrios EQ, Beckman Coulter, Inc., CA, USA). Among these, the IgG homotypic control antibody information corresponding to CD29, CD34, CD44, and CD45 were Armenian Hamster IgG Isotype Control (eBio299Arm) [PE-Cyanine7] (25-4888-82, eBioscienceB), Mouse IgG1 Isotype Control (11711) [Alexa Fluor® 488] (IC002G, Novus Biologicals), Mouse IgG2a kappa Isotype Control (eBM2a) [PE] (12-4724-82, eBioscience™) and Mouse IgG1 kappa Isotype Control (P3.6.2.8.1) [FITC] (11-4714-81, eBioscience™).

2.11. Culture of BMSCs with scaffold extract

2.11.1. 3-(4,5-Dimethylthiazol-2-yl)-2,5-diphenyltetrazolium bromide (MTT) assay

The subcultured BMSCs at the 3rd generation were seeded in 24-well plates containing scaffold samples at 1×10^5 cells/well and incubated at 37 °C with 5% CO$_2$, with the low-glucose DMEM containing 10% FBS as the negative control group (control group). The medium was refreshed every 3 d, for a total of 14 d. On the 1st, 3rd, and 7th d of culture, scaffolds were removed out and rinsed with PBS twice, and 10 μL MTT solution (Sigma Aldrich, St. Louis, MO, USA) reagent was added into each well of the culture plates and incubated at 37 °C for 4 h, and the reaction was terminated with dimethyl sulfoxide (DMSO) according to the instructions. The optical density (OD) value at 570 nm was measured using a microplate reader. The relative survival rate of cells of each group = (average OD value of experimental group/average OD value of negative control group) $\times$ 100%.

2.11.2. Osteogenic induction differentiation of BMSCs

The subcultured BMSCs at the 3rd generation were seeded in 24-well plates containing scaffold samples at 1×10^5 cells/well and incubated at 37 °C with 5% CO$_2$, with the DMEM containing osteogenic induction medium (OIM), 10% FBS, 10^{-8} mol/L dexamethasone, 50 μg/mL vitamin C, and 10 mmol/L β-GP. The medium was refreshed every 3 d, for a total of 14 d. After culture for 3 days, scaffolds were removed out and rinsed with PBS twice.

2.11.3. Alkaline phosphatase (ALP) activity determination

On the 3rd, 7th, and 14th days of osteogenic induction differentiation of BMSCs in each group, the ALP activity of cell lysate was

detected using the ALP Colorimetric Assay Kit (E-BC-K091-S, Elabscience, Wuhan, Hubei, China) according to the instructions.

2.11.4. ALP staining

On the 3rd, 7th, and 14th d of osteogenic induction differentiation of the BMSCs in each group, the cells were stained using the ALP staining kit (Biotides, Beijing, China) under the instructions.

2.11.5. Western blot

The BMSCs on the 14th d of the incubation with scaffolds and on the 14th d of osteogenic induction differentiation were collected and lysed with radio-immunoprecipitation assay (RIPA) lysate, and the protein concentration of the lysate was determined using the bicinchoninic acid (BCA) Protein Assay kit (Sangon Biotech, Shanghai, China). The 40 μg protein was isolated on the 10% sodium dodecyl sulfate-polyacrylamide gel electrophoresis, transferred on the polyvinylidene fluoride membranes (240 mA, 4 h), sealed with 5% skim milk, washed with tris buffered saline-Tween20 (TBST) buffer solution 3 times, and incubated with primary antibodies (Collagen I antibody, ab270993, 1:1000, 139 kDa, Abcam, Cambridge, MA, USA; Osteocalcin antibody, PA5-86886, 1:1000, 11 kDa, Invitrogen, Carlsbad, CA, USA; Osteopontin antibody, PA5-34579, 1 μg/mL, 35 kDa, Invitrogen) at 4 °C overnight. After that, the samples were washed with TBST 3 times and incubated with horseradish peroxidase-labeled goat anti-rabbit IgG (1:5000, ab205718) at room temperature for 1 h. With GAPDH (1:10000, 36KD, ab181602) as the internal reference, the bands were visualized by chemiluminescence and analyzed using an imager.

2.11.6. Statistical analysis

Data were analyzed using GraphPad Prism 8.01 (GraphPad Software Inc., San Diego, CA, USA) and SPSS 21.0 (IBM Corp. Armonk, NY, USA), and the results were expressed as mean ± standard deviation. The comparisons between the two groups were conducted using *t*-test, and comparisons among groups were conducted using one-way analysis of variance (ANOVA), followed by Tukey's test. *P* value was obtained by a bilateral test. $P < 0.05$ indicated statistical significance.

3. Results

3.1. Characterization of low-temperature 3D printing PLGA/MgO scaffolds

a. Macro and microstructure evaluation of scaffolds

The actual appearance of the scaffolds was shown in Fig. 1A. SEM images of scaffolds in the PLGA group and PLGA/MgO (10%) group were shown in Fig. 1B. The scaffolds in both groups had uniform material structure and smooth duct structure. The surface of PLGA scaffolds was smooth, while the compactness of the surface of PLGA/MgO (10%) scaffolds was increased. The line diameter of each scaffold with different MgO ratios (5%, 10%, and 15%) was 600–650 μm, and the pore size was 460 μm. The porosity of scaffolds in each group calculated by the ethanol replacement method was more than 80%, and there was no significant difference among the groups (Table 1). The surface chemical functional groups of scaffolds were analyzed by infrared spectroscopy (Fig. 1C). The absorption bands of scaffolds in each group mainly appeared in 2990 cm^{-1} and 2940 cm^{-1} (-CH3), and 1753 cm^{-1}, 1183 cm^{-1} and 1083 cm^{-1} (C=O). The EDS analysis results of scaffolds were shown in Fig. 1D. Magnesium (Mg), carbon (C), and oxygen (O) were detected from all the PLGA/MgO scaffolds and the PLGA/MgO/PDA scaffolds. Nitrogen(N) was also detected from all the PLGA/MgO/PDA scaffolds. The water contact angle test results elicited that with

the increase of MgO content, the water contact angle of the scaffold material was gradually decreased and the hydrophilicity of the material was increased (Fig. 1E).

b. Evaluation of scaffold mechanical properties

The effects of MgO content on scaffold mechanical properties were further studied. Compared with the PLGA group, the PLGA/MgO (10%) scaffolds showed increased compressive strength and elastic modulus, which were also higher than those of the scaffolds with the MgO content of 5% or 15% (Fig. 2).

c. Evaluation of scaffold degradation *in vitro*

To study the degradation rate and the magnesium ion release rate of PLGA scaffolds with different MgO contents, the *in vitro* scaffold degradation and magnesium ion were detected. The *in vitro* degradation test results were shown in Fig. 3A. With the extension of time, the scaffolds in each group were degraded. There were significant differences among the 4 groups (all $P < 0.05$). The degradation rate was accelerated with the increase of MgO content, but there was no significant difference between the PLGA/MgO (10%) group and the PLGA/MgO (15%) group. As shown in Fig. 3B, the magnesium ion release of MgO-containing scaffolds tended to be flat after 21 d. With the increase of MgO content, the magnesium ion release concentration was increased (all $P < 0.05$). As shown in Fig. 3C, the pH value of the PLGA scaffold extract was decreased slowly, while the pH values of the 3 groups of MgO-containing scaffold extracts were higher than that of the PLGA group on the 1st, 3rd and 7th d, indicating that the release of magnesium ions could alleviate the decrease of pH value caused by PLGA degradation, with higher MgO content exerting the stronger effect (all $P < 0.05$). After the 28th d, the pH value of the extract of PLGA/MgO scaffolds in the 3 groups was higher than that of the PLGA scaffolds (all $P < 0.05$).

3.2. Biocompatibility of low-temperature 3D printing PLGA/MgO scaffolds

a. Cytotoxicity

The morphology of BMSC was observed under a phase-contrast microscope. After 24 h of the passage, the cells adhered to the wall completely. The cell morphology was uniform, typical spindled shape, and the cell colonies were arranged in a vortex or radial shape (Fig. 4A). The results of flow cytometry elicited that the cultured BMSCs of the 3rd generation expressed CD29 and CD44, and the positive rates were 97.652% and 98.917%, respectively, while CD34 and CD45 were negative, and the positive rates were 0.013% and 0.108%, respectively (Fig. 4B). To investigate the toxicity of scaffolds in each group to rat BMSCs, MTT assay showed that the relative survival rates of cells in other groups were more than 75% within 14 d except the PLGA/MgO (15%) group (Fig. 4C and D). According to the regulations of ISO10993-5, the relative proliferation of cells ≥75% was in the qualified range, indicating that MgO could inhibit the survival of cells when the proportion reached 15%.

b. Osteogenesis

To study the effect of scaffold materials on the osteogenic activity of BMSCs, the ALP activity of BMSCs induced by osteogenesis after 1, 7, and 14 d of incubation with scaffold extract was detected. The ALP activity of the 4 groups of cells was increased with the extension of time, indicating that these 4 scaffolds could support the osteogenic differentiation of BMSCs. After 7 and 14 d of culture, the ALP activity
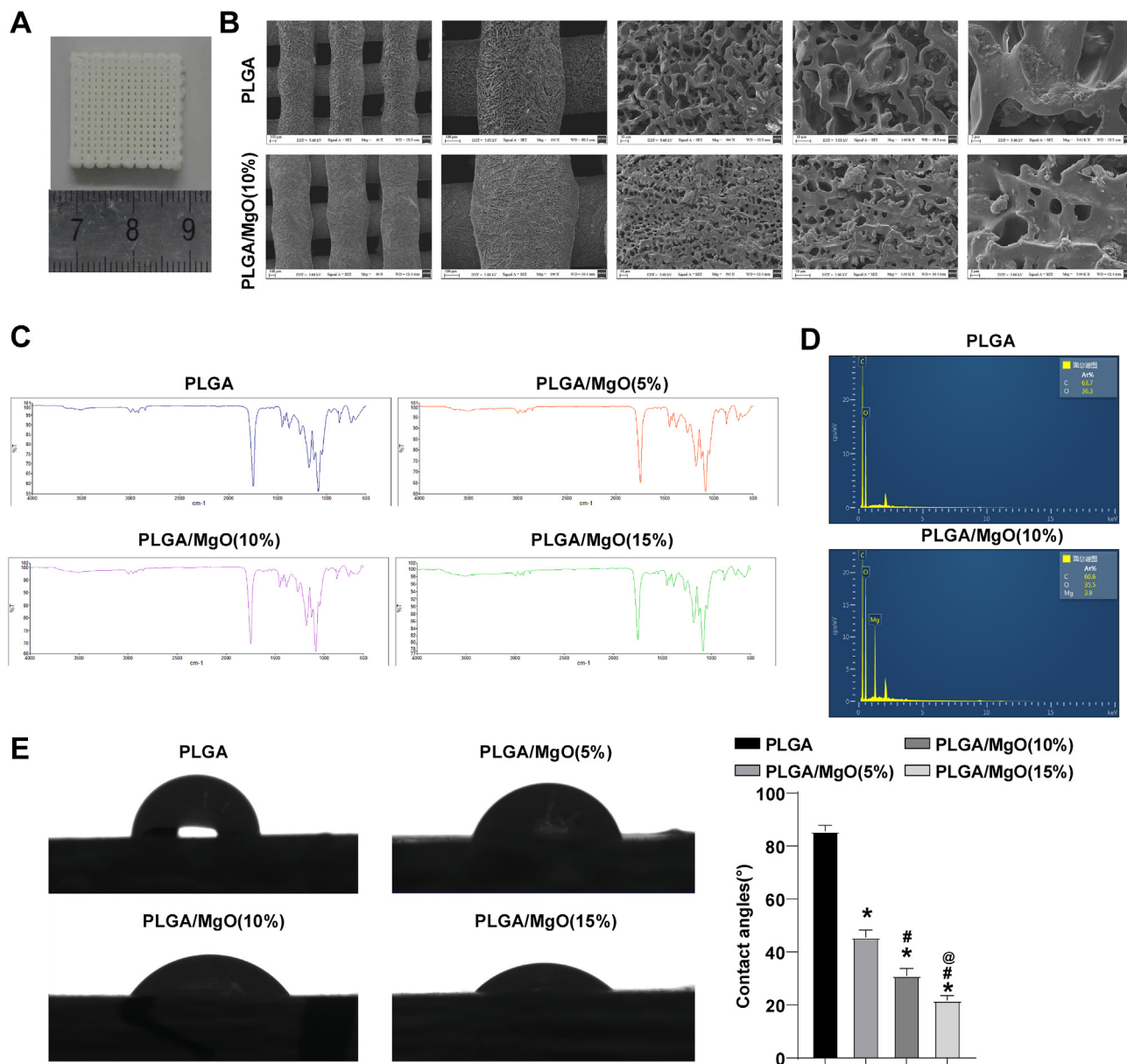
Fig. 1. Macro and microstructure evaluation of scaffolds. Low-temperature 3D printing PLGA scaffolds and PLGA/MgO scaffolds with different magnesium mass ratios were compared. (A) Actual image of scaffolds; (B) SEM images of scaffolds; (C) Detection of chemical functional groups of scaffolds by infrared spectrometer; (D) XPS spectra of different scaffold surfaces; (E) Hydrophilicity of scaffolds was detected by water contact angle meter. The 6 samples were detected for each kind of the scaffolds. The data in panel E were expressed as mean ± standard deviation. One-way analysis of variance (ANOVA) was employed for comparisons among groups, followed by Tukey's multiple comparisons test. * Compared with the PLGA group, $P < 0.05$, # compared with the PLGA/MgO (5%) group, $P < 0.05$, @ compared with the PLGA/MgO (10%) group, $P < 0.05$.

Table 1
Structural characteristics of PLGA/MgO scaffolds.

Scaffolds category	Line diameter (μm)	Aperture (μm)	Porosity (%)
PLGA	602.1 ± 32.3	452.3 ± 41.5	83.2 ± 1.7
PLGA/MgO (5%)	617.6 ± 35.8	461.3 ± 39.0	83.8 ± 2.1
PLGA/MgO (10%)	647.0 ± 37.6	461.4 ± 44.9	83.6 ± 3.6
PLGA/MgO (15%)	626.8 ± 37.4	465.7 ± 43.0	81.8 ± 3.9
P value	0.211	0.974	0.779

Note: One-way ANOVA was employed to analyze the differences of line diameter, aperture and porosity among multiple groups.

of the PLGA/MgO (10%) group was higher than that of the other 3 groups (Fig. 5A, all $P < 0.05$), indicating that it could more effectively promote the osteogenic differentiation of BMSCs. The results of ALP

staining were consistent with the above results (Fig. 5B). Western blot demonstrated that the expressions of collagen I, Osteocalcin, and Osteopontin proteins in the PLGA/MgO (10%) group were higher than those in other groups (Fig. 5C, all $P < 0.05$). The above results suggested that PLGA/MgO (10%) scaffolds were the most conducive to the osteogenic differentiation of BMSCs.

3.3. Characterization of low-temperature 3D printing PLGA/MgO/ PDA scaffolds

a. Macro and microstructure evaluation of scaffolds

According to the previous results, compared with PLGA/MgO (5%) and PLGA/MgO (15%) scaffolds, PLGA/MgO (10%) scaffolds had
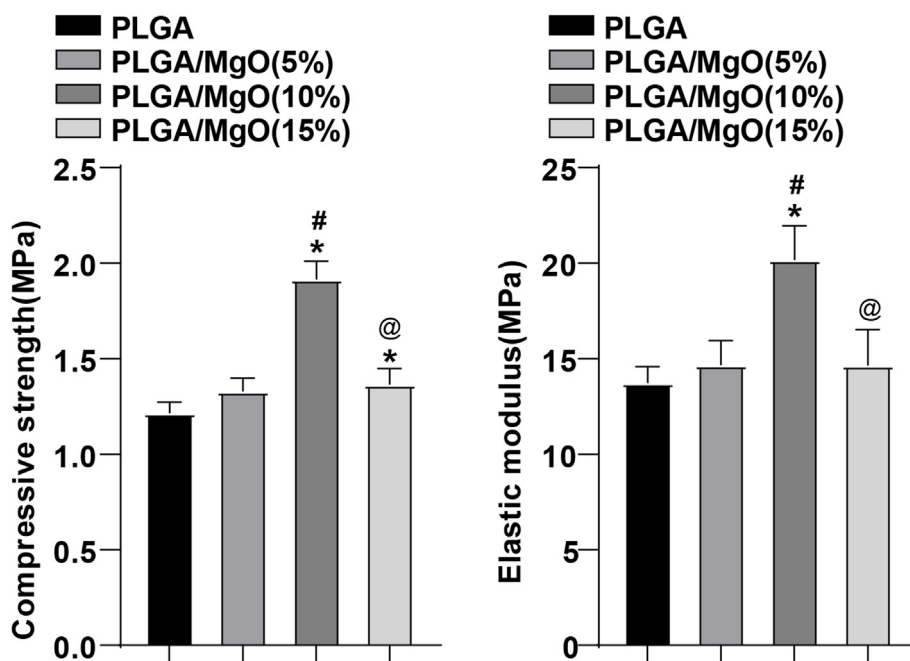
Fig. 2. Comparison of mechanical properties of scaffolds with different magnesium contents. The compressive strength and elastic modulus of PLGA scaffolds and PLGA/MgO scaffolds were measured using a universal mechanical tester. The 6 samples were detected for each kind of the scaffolds. The data were expressed as mean ± standard deviation. One-way ANOVA was employed for comparisons among groups, followed by Tukey's multiple comparisons test. * Compared with the PLGA group, $P < 0.05$, # compared with the PLGA/MgO (5%) group, $P < 0.05$, @ compared with the PLGA/MgO (10%) group, $P < 0.05$.
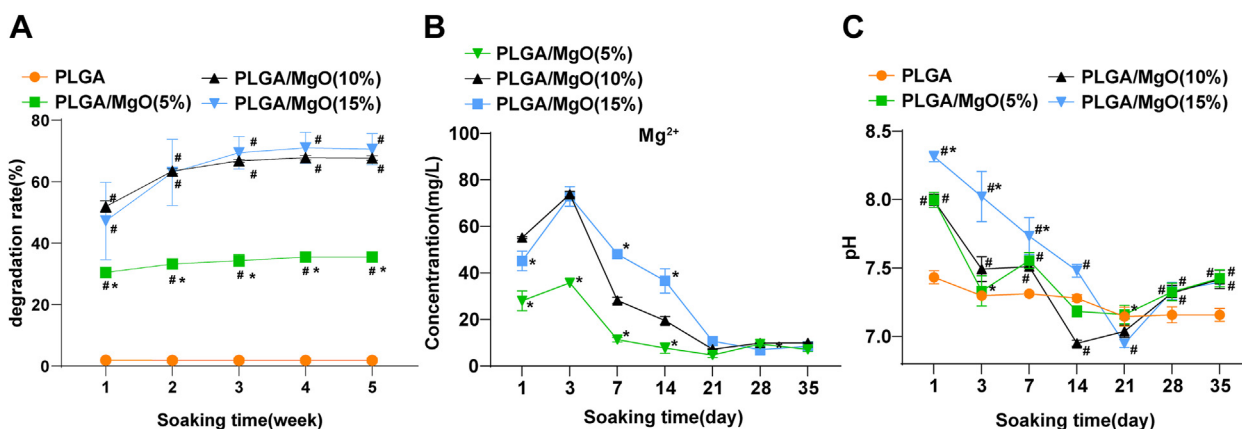

Fig. 3. Degradation properties of PLGA/MgO scaffolds. The scaffold materials were placed in PBS to determine the degradation properties *in vitro*. (A) The change curve of degradation rate; (B) The change curve of magnesium ion release *in vitro*; (C) pH change curve of scaffolds *in vitro*. The 4 samples were detected for each kind of the scaffolds. The data were expressed as mean ± standard deviation. One-way ANOVA was employed for comparisons among groups, followed by Tukey's multiple comparisons test. * Compared with the PLGA/MgO (10%) group, $P < 0.05$, # compared with the PLGA group, $P < 0.05$.

better mechanical properties and osteogenic ability, and less cytotoxicity. Therefore, PLGA/MgO (10%) scaffolds were selected for PDA coating treatment to obtain PLGA/MgO (10%)/PDA scaffolds, and their properties were compared with the PLGA/MgO (10%) scaffolds.

The actual image and SEM image of 2 two scaffolds (Fig. 6A and B) showed that the duct structures of the 2 scaffolds were through, and evenly distributed MgO particles could be seen in the 2 groups of scaffolds. Compared with PLGA/MgO (10%) scaffolds, the surface of PLGA/MgO (10%)/PDA scaffolds formed a thin film coating, and the micro surface was uneven. The line diameter of each group of scaffolds was about 620−640 μm and the aperture approx was 460−480 μm. The porosity calculated by the ethanol replacement method was more than 80% (Table 2). New bands were observed in

the infrared spectra of PLGA/MgO (10%)/PDA scaffolds at 1632 cm^{-1} and 3000−3600 cm^{-1} (Fig. 6C), indicating that PDA was successfully coated on both scaffolds. As shown in Fig. 6D, the nitrogen signal of the PLGA/MgO (10%)/PDA scaffold was significantly enhanced. The results of the water contact angle experiment elicited that the hydrophilicity of the PLGA/MgO (10%)/PDA scaffold was better than that of PLGA/MgO (10%) (Fig. 6E, $P < 0.05$).

b. Evaluation of scaffold properties and biocompatibility

The mechanical properties of the 2 scaffolds were compared. There were no significant differences in compressive strength and elastic modulus between PDA-coated scaffolds and PLGA/MgO (10%) scaffolds (Fig. 7A and B). PDA is helpful to reduce the
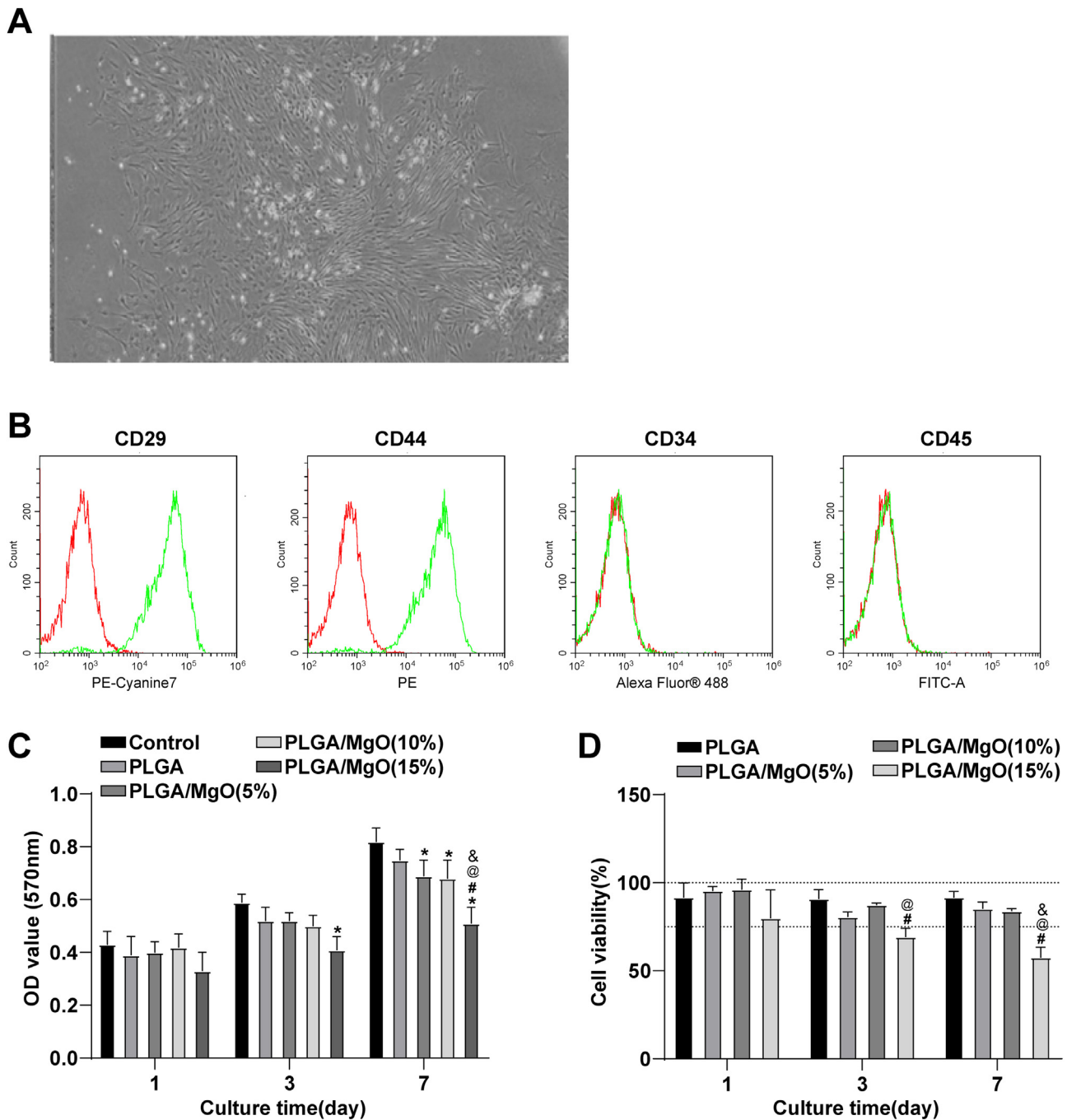
Fig. 4. Cytotoxicity of PLGA/MgO scaffold on rat BMSCs. The scaffold extract was prepared from each group of scaffolds and co-incubated with BMSCs. (A) The morphological characteristics of BMSCs were observed under a phase-contrast microscope; (B) The expression of surface markers of BMSCs was detected by flow cytometry. IgG was used as the homotypic negative control, with a negative rate of 100% (red curve); (C) The OD value of BMSCs in each group after MTT staining; (D) The relative survival rate of cells in each group was determined by MTT assay. The cell experiment was repeated 3 times independently. The data were expressed as mean ± standard deviation. One-way ANOVA was employed for comparisons among groups, followed by Tukey's multiple comparisons test. * Compared with the control group, $P < 0.05$, # compared with the PLGA group, $P < 0.05$, @ compared with the PLGA/MgO (5%) group, $P < 0.05$, & compared with the PLGA/MgO (10%) group, $P < 0.05$.

corrosion rate of magnesium alloys and regulate the release of magnesium ions. The *in vitro* degradation properties of PLGA/MgO (10%)/PDA scaffolds were analyzed. The degradation rate of PLGA/MgO (10%)/PDA scaffolds was lower than that of the PLGA/MgO (10%) scaffolds (Fig. 7, all $P < 0.05$), the release concentration of magnesium ions was lower (Fig. 7D, all $P < 0.05$), the pH value was decreased more slowly and was higher than that of the PLGA/MgO (10%) scaffolds on the 3rd, 14th and 21st d (Fig. 7E, all $P < 0.05$). It

suggested that PDA coating could delay scaffold degradation and magnesium ion release. To evaluate the cytotoxicity of PLGA/MgO (10%)/PDA scaffolds, MTT assay was conducted. The results demonstrated that the relative survival rate of cells in this group was increased (Fig. 7F and G), suggesting that PLGA/MgO (10%)/PDA scaffolds had better biosafety. In addition, the effects of scaffolds coated with PDA on the osteogenic activity of BMSCs were compared. The results showed that the ALP activity in the PLGA/
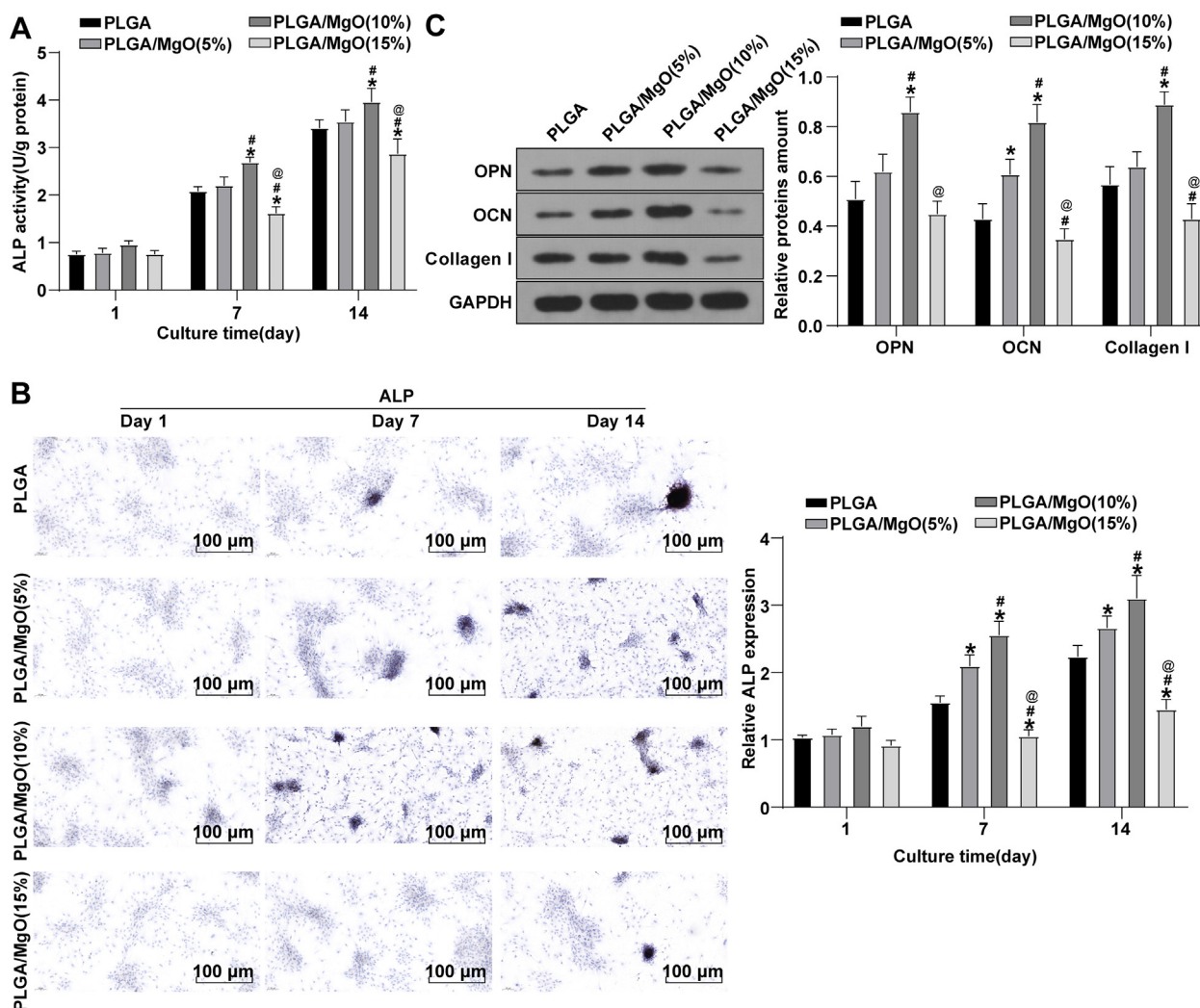
Fig. 5. Effects of PLGA/MgO scaffolds on osteogenic differentiation of rat BMSCs. BMSCs were incubated with scaffold extract for 1, 7, and 14 d, and then induced by osteogenic differentiation. (A) ALP activity was measured by colorimetry; (B) ALP staining and quantitative analysis of cells in each group (the left graph panel showed representative images of ALP staining of BMSCs incubated with each group of scaffold extracts for 1, 7, and 14 days, and the right graph showed the results of the ALP quantitative analysis); (C) The expressions of OPN, OCN, and Collagen I after 14 d of incubation with scaffold extract were detected by Western blot. The experiment was repeated 3 times independently. The data were expressed as mean ± standard deviation. One-way ANOVA was employed for comparisons among groups, followed by Tukey's multiple comparisons test. * Compared with the PLGA group, $P < 0.05$, # compared with the PLGA/MgO (5%) group, $P < 0.05$, @ compared with the PLGA/MgO (10%) group, $P < 0.05$.

MgO (10%)/PDA group was higher than that of the PLGA/MgO (10%) group (Fig. 7H, all $P < 0.05$), and it was consistent with the ALP staining results (Fig. 7I). Western blot elicited that the expressions of Osteocalcin, Osteopontin, and Collagen I proteins in the PLGA/MgO (10%)/PDA group were higher than those in the PLGA/MgO (10%) group (Fig. 7J, all $P < 0.05$). The above results suggested that the addition of PDA coating in PLGA/MgO (10%) was beneficial to reducing the cytotoxicity of scaffolds and inducing osteogenic differentiation of BMSCs.

4. Discussion

Bone tissues have multiple effects on day-to-day functionality and the frequency of accidental bone disorder and damage is increasing all over the world [29]. Evidence has shown that 3D printing can produce efficient scaffolds, which are highly desirable for bone tissue engineering [6]. This study found that low-temperature 3D printing PLGA/MgO (10%)/PDA scaffolds had good hydrophilicity and biocompatibility and were conducive to BMSC osteogenic differentiation.

3D printing of bone scaffolds is a promising method as it combines the accuracy of 3D printing technology and tissue engineering to manufacturing bionic bone implants with an ideal shape and internal structure [30]. In this study, a low-temperature 3D printing technology was used, which was carried out at a low temperature and had little impact on the bioactivity of the factors contained in the scaffold. In contrast with the printed scaffolds incubated in a muffle furnace at 150 °C to promote cross-linking, which will destroy incorporated growth factor biological activity, the printed scaffolds fabricated at a low temperature show minimally affected biological activity [31].

PLGA is a synthetic lipophilic polymer material, which is widely used in the research of tissue engineering bone repair materials, but the mechanical properties are poor [13]. The mechanical properties of an ideal bone scaffold should match the properties of autologous bone [32]. Magnesium and its alloys are considered a promising biomaterial for bone regeneration due to their inherent biocompatibility, biodegradability, and the appropriate elastic modulus close to that of bone (bone:3–20 GPa, magnesium:41–45 GPa) [33]. It is reported that the strength of Mg
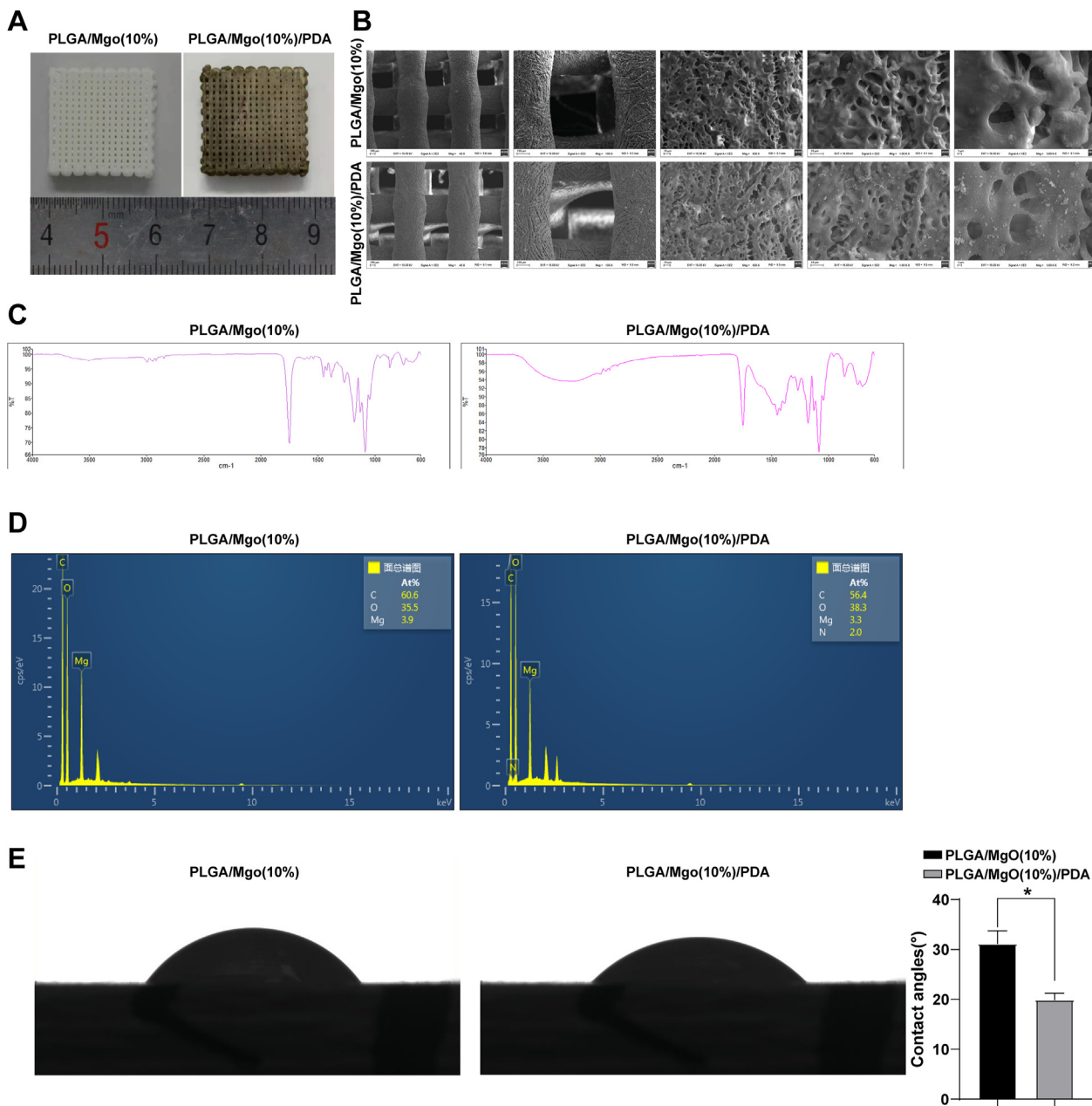
Fig. 6. Macro and microstructure evaluation of PLGA/MgO/PDA scaffolds. PLGA/MgO (10%)/PDA scaffolds were prepared and characterized. (A) Physical image and (B) SEM image of PLGA/MgO (10%)/PDA scaffolds. The arrow indicated that PDA formed a thin film coating on the surface of the scaffolds; (C) The chemical functional groups of the scaffolds were detected by infrared spectrometer; (D) X-ray photoelectron spectroscopy analysis of scaffolds; (E) The hydrophilicity of the scaffold was detected by water contact angle meter. The 6 samples were detected for each kind of the scaffolds. The data in panel E were expressed as mean ± standard deviation. Independent t-test was employed for comparisons among groups. *$P < 0.05$.

Table 2
Structural characteristics of PLGA/MgO/PDA scaffolds.

Scaffolds category	Line diameter (μm)	Aperture (μm)	Porosity (%)
PLGA/MgO (10%)	647.0 ± 37.6	461.4 ± 44.9	83.6 ± 3.6
PLGA/MgO (10%)/PDA	624.8 ± 39.2	488.4 ± 43.9	84.0 ± 4.6
P value	0.34	0.423	0.908

Note: Independent t-test was employed to analyze the differences of line diameter, aperture and porosity among multiple groups.

is 16 times that of polymer, and they are more ductile than ceramics [34]. Therefore, adding magnesium powder can improve the mechanical properties of polymers and neutralize the rigidity of ceramics. We fabricated 3 kinds of scaffolds with different proportions of MgO (5%, 10%, 15%). Mechanical properties including contact angle, tensile strength, compressive strength, and elastic modulus are used to determine the mechanical and physical properties of the scaffold [35]. Our results elicited that when the MgO ratio reached 10%, the compactness of the material surface had a higher density, the scaffold material had a smaller water contact angle, and the material had a higher hydrophilicity, compressive strength, and elastic modulus; It is consistent with that coaxial-MgO with the core-shell fiber structure has a better property of hydrophilicity [36]. Consistently, MgO with good bioactivity is beneficial to improving polylactide (PLA) biocompatibility and mechanical properties during the bone repair
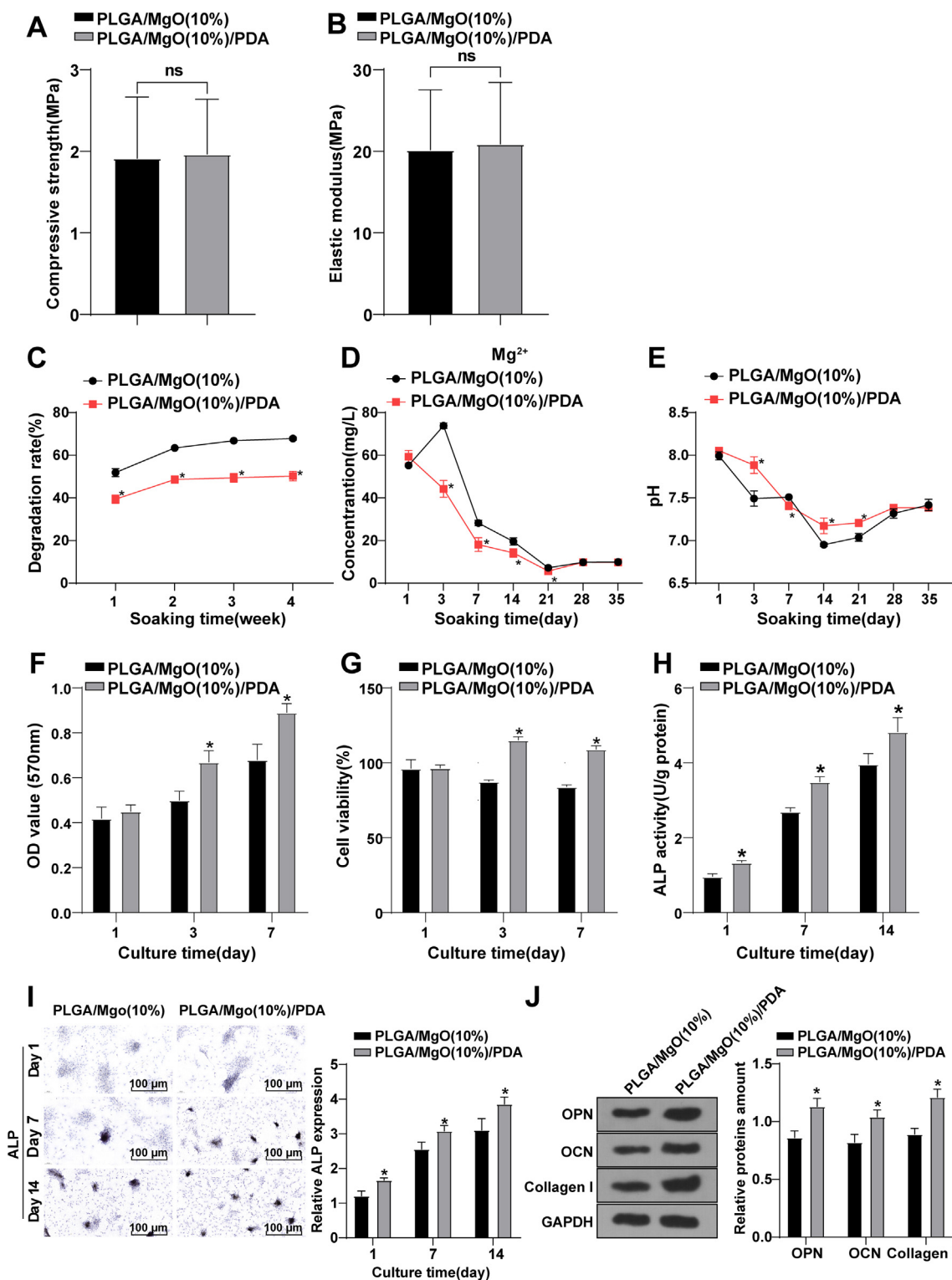
Fig. 7. Properties and biocompatibility evaluation of PLGA/MgO (10%)/PDA scaffolds. The compressive strength (A) and elastic modulus (B) of PLGA/MgO (10%) scaffolds and PLGA/MgO (10%)/PDA scaffolds was measured by universal mechanical testing machine. The 6 samples of each kind of scaffolds were selected for measurement. PLGA/MgO (10%)/PDA scaffolds were placed in PBS to determine the change curve of mass loss percentage during scaffold degradation (C), the change curve of magnesium ion release *in vitro* (D) and the change curve of pH value *in vitro* (E); The scaffold extract was prepared and co-incubated with BMSCs. The OD values (F) and relative survival rates (G) of BMSCs after MTT staining were measured. The ALP activity (H) and ALP staining quantitative analysis (the left graph panel showed representative images of ALP staining of BMSCs incubated with each group of scaffold extracts for 1, 7, and 14 days, and the right graph showed the results of the ALP quantitative analysis) (I) were measured by colorimetry. The expressions of OPN, OCN and Collagen I proteins in cells 14 d after scaffold inoculation was detected by Western blot (J). The cell experiment was repeated 3 times. Independent *t*-test was employed for comparisons among groups. ns: *P* > 0.05, * compared with the PLGA/MgO (10%) group, *P* < 0.05.

process [37]. The implanted scaffolds will degrade gradually along with tissue regeneration [38]. To maintain functionality, the implant degradation rate should be closely balanced by neo-tissue formation [39]. Our results revealed that the degradation rate was accelerated with the increase of MgO content, but there was no significant difference between scaffolds with 10% and 15% MgO contents. It has been reported that compared to the PLGA/trical-cium phosphate (TCP) scaffolds, PLGA/TCP/Mg scaffolds degrade faster due to magnesium corrosion [40]. Our results were consistent with this, and the increase in degradation rate caused by the addition of MgO might also be due to magnesium corrosion. After transplantation, the magnesium ions released by the PLGA/MgO scaffolds might mediate the differentiation of BMSCs into osteoblasts by regulating BMP2 levels, thereby increasing their impact on bone defect repair. With the increase of MgO content, the magnesium ion release concentration was increased and the pH values of the MgO-containing scaffold extracts were higher than those of the PLGA scaffold extract, which suggested that magnesium ion release alleviated the decrease of pH value caused by PLGA degradation, with higher MgO content exerting the stronger effect. Magnesium ions are bioactive and can promote the regeneration of bone tissues, in which the enhancing efficiency is closely associated with magnesium ion concentration [21]. With the addition of MgO, the pH values of the degrading solution were higher through the neutralization of the acidic product of the PLA degradation [41]. Specifically, in our results, there were three groups of magnesium containing scaffold extracts with pH values equal to or even lower than those of the PLGA control sample added on the 21st day. A reasonable explanation might be as below: the acidic degradation of PLGA and the self-accelerating effect during the degradation process gradually increased from day 14—21, and reached its maximum on day 21. However, the release of magnesium ions was in a rapidly decreasing state on day 14—21. On day 21, the accumulated release of magnesium ions might not be sufficient to compensate for the pH decrease caused by acidic degradation. After 21 days, the acidic degradation of PLGA and the self-accelerating effect during the degradation process slowed down, and the release of accumulated magnesium ions showed a alleviating effect on the decrease caused by PLGA degradation. In addition, research has reported that continuous local hyperacidity conditions can affect osteoblast activity and inhibit osteoblast proliferation [42], while the establishment of a weakly alkaline environment is conducive to osteoblast growth [43]. In our results, although the pH value of the PLGA/MgO (15%) scaffold extract with high magnesium content might shift towards alkaline direction (pH > 8.0 on days 1 and 3), it tended to reach a level of 7.5 in the long run. Therefore, we believe that this should be beneficial for the growth of osteoblasts. Collectively, PLGA/MgO (10%) scaffolds had strong mechanical properties and high degradation rates.

The primary goal of developing bone repair materials is to repair defective bone tissues, and the performance of the scaffold relys on its osteogenic ability [40,44—46]. ALP is used to characterize osteogenic differentiation [47]. Our results demonstrated that the ALP activity in BMSCs cultured with PLGA/MgO (10%) scaffold extract was the highest, which suggested that it could more effectively promote BMSC osteogenic differentiation. Collagen I, Osteocalcin, and Osteopontin are the osteogenic genes [48]. Collagen can be crosslinked with chemicals and provides great tensile strength in tissues and as a scaffold, collagen allows for easy placement of stem cells and allows for replacement with natural tissues after undergoing degradation [4]. The expressions of collagen I, Osteocalcin, and Osteopontin protein in the BMSCs cultured with PLGA/MgO (10%) scaffold extract were the highest. Accumulating evidence has

repeatedly shown the bioregulatory importance of Mg ions in ALP activity and MSC growth and osteogenic differentiation [49]. In conclusion, PLGA/MgO (10%) scaffolds had better hydrophilicity, mechanical properties, osteogenic ability, and less cytotoxicity. Therefore, PLGA/MgO (10%) scaffolds were selected for PDA coating treatment.

PDA is used to modify the surface of the scaffolds, which can regulate the release of magnesium ions [50]. We coated PLGA/MgO(10%) scaffolds with PDA and found that the nitrogen signal of PLGA/MgO(10%)/PDA was enhanced, the hydrophilicity of PLGA/MgO (10%)/PDA scaffolds was better than that of the PLGA/MgO (10%) scaffolds. Consistently, PDA coating improves hydrophilicity and causes an increase in metabolic activity and attachment of in vitro mammalian cells [51]. We then compared the mechanical property of the 2 kinds of scaffolds and found that there were no differences in compressive strength and elastic modulus between PDA-coated scaffolds and PLGA/MgO (10%) scaffolds. Besides, our results revealed that the degradation rate of PLGA/MgO (10%)/PDA scaffold was decreased, magnesium ion release concentration was diminished, and the reduction in pH value was delayed, indicating that PDA coating delayed magnesium ion release and scaffold degradation; the relative survival rate of cells was increased, indicating better biosafety. Furthermore, the ALP activity in BMSCs cultured with PLGA/MgO (10%)/PDA extract was increased; the expression levels of Osteocalcin, Osteopontin, and Collagen I were enhanced. In a similar light, PDA-BCP scaffold facilitates the viability, adhesive and proliferative properties and new bone formation of BMSCs which is associated with the nanostructure, superhydrophilicity and other properties of PDA [26]. Moreover, PDA coating further promotes cell adhesion due to enhanced adsorption of serum proteins [52]. Polycaprolactone scaffold coated with PDA makes a difference in cell proliferation and osteoconductivity [53]. The calcium phosphate/PDA coating has a nano-scale porous topography, which is good for BMSCs behavior and osteogenesis in vivo [54]. PDA/graphene oxide composite stimulates ALP activity and osteogenic differentiation of pluripotent embryonic stem cells [55]. Tantalum-PDA-Mg2 shows the highest ion release and excellent biocompatibility, adhesion, angiogenesis, and osteogenesis [56]. Although magnesium alloys are applied as biodegradable biomaterials for medical device production, their use is restricted because of the high degradation rate, and a PDA layer can increase the adhesion between the external organic coating and metallic substrate and decrease the substrate degradation rate [57]. Our findings also manifested that PDA coating in PLGA/MgO (10%) scaffolds reduced the cytotoxicity of scaffolds and promoted osteogenic differentiation of BMSCs.

In summary, this study supported that low-temperature 3D printing PLGA/MgO (10%)/PDA scaffolds had good hydrophilicity and biocompatibility, and were conducive to BMSC osteogenic differentiation. The compressive strength of PLGA/MgO scaffolds was 1.92 MPa and the elastic modulus was 20.20 Mpa, which was expected to be used in the field of load-bearing bone defect repair. The degradation rate and cytotoxicity of the scaffolds were controlled by adjusting the content of MgO to obtain better biocompatibility. The scaffolds coated with PDA had improved bioactivity and reduced cytotoxicity and facilitated the osteogenic differentiation of BMSCs. However, the composite scaffolds were not verified in vivo and in clinical experiments. Further work is needed to improve the preparation method of PDA/MgO printing ink to improve the fluidity and uniformity, and the scale needs to be expanded. Further study of mechanical decay and osteogenic activity of PDA/MgO/PDA scaffolds in vivo is needed.

Ethics statement

All procedures were authorized by the academic ethics committee of Shenzhen Hospital, Southern Medical University. All the laboratory procedures were used to reduce the pain of the rats. The animal experiments have been carried out in accordance with the ARRIVE guidelines.

Consent for publication

Not applicable.

Availability of data and materials

The data that support the findings of this study are available from the corresponding author upon reasonable request.

Funding

Authors' contributions

LT is the guarantor of integrity of the entire study and contributed to the study design; ZFY, WDZ contributed to the definition of intellectual content, manuscript editing; BNM, HTL contributed to the study concepts, data analysis; XWL contributed to the literature research, manuscript preparation; JCW contributed to the data acquisition, statistical analysis; HXS contributed to the study concepts, manuscript review; All authors read and approved the final manuscript.

Declaration of competing interest

The authors declare that they have no known competing financial interests or personal relationships that could have appeared to influence the work reported in this paper.

Acknowledgements

Not applicable.

Appendix A. Supplementary data

Supplementary data to this article can be found online at https://doi.org/10.1016/j.reth.2023.09.015.

References

[1] Bahraminasab M. Challenges on optimization of 3D-printed bone scaffolds. Biomed Eng Online 2020;19:69.
[2] Forrestal DP, Klein TJ, Woodruff MA. Challenges in engineering large customized bone constructs. Biotechnol Bioeng 2017;114:1129−39.
[3] Yamauchi N, Yamauchi S, Nagaoka H, et al. Tissue engineering strategies for immature teeth with apical periodontitis. J Endod 2011;37:390−7.
[4] Gathani KM, Raghavendra SS. Scaffolds in regenerative endodontics: a review. Dent Res J 2016;13:379−86.
[5] Wang B, Chariyev-Prinz F, Burdis R, Eichholz K, Kelly DJ. Additive manufacturing of cartilage-mimetic scaffolds as off-the-shelf implants for joint regeneration. Biofabrication 2022;14.

[6] Wang C, Huang W, Zhou Y, et al. 3D printing of bone tissue engineering scaffolds. Bioact Mater 2020;5:82−91.
[7] Iglesias-Mejuto A, Garcia-Gonzalez CA. 3D-printed alginate-hydroxyapatite aerogel scaffolds for bone tissue engineering. Mater Sci Eng C 2021;131: 112525.
[8] Pan T, Song W, Xin H, et al. MicroRNA-activated hydrogel scaffold generated by 3D printing accelerates bone regeneration. Bioact Mater 2022;10:1−14.
[9] Domingos M, Intranuovo F, Gloria A, et al. Improved osteoblast cell affinity on plasma-modified 3-D extruded PCL scaffolds. Acta Biomater 2013;9: 5997−6005.
[10] Wang T, Zheng J, Hu T, et al. Three-dimensional printing of calcium carbonate/hydroxyapatite scaffolds at low temperature for bone tissue engineering. 3D Print Addit Manuf 2021;8:1−13.
[11] Wen Y, Xun S, Haoye M, et al. 3D printed porous ceramic scaffolds for bone tissue engineering: a review. Biomater Sci 2017;5:1690−8.
[12] Ngiam M, Liao S, Patil AJ, Cheng Z, Chan CK, Ramakrishna S. The fabrication of nano-hydroxyapatite on PLGA and PLGA/collagen nanofibrous composite scaffolds and their effects in osteoblastic behavior for bone tissue engineering. Bone 2009;45:4−16.
[13] Yan B, Zhang Z, Wang X, et al. PLGA-PTMC-Cultured bone mesenchymal stem cell scaffold enhances cartilage regeneration in tissue-engineered tracheal transplantation. Artif Organs 2017;41:461−9.
[14] Mantripragada VP, Lecka-Czernik B, Ebraheim NA, Jayasuriya AC. An overview of recent advances in designing orthopedic and craniofacial implants. J Biomed Mater Res 2013;101:3349−64.
[15] Hickey DJ, Ercan B, Sun L, Webster TJ. Adding MgO nanoparticles to hydroxyapatite-PLLA nanocomposites for improved bone tissue engineering applications. Acta Biomater 2015;14:175−84.
[16] Roh HS, Lee CM, Hwang YH, et al. Addition of MgO nanoparticles and plasma surface treatment of three-dimensional printed polycaprolactone/hydroxyapatite scaffolds for improving bone regeneration. Mater Sci Eng C 2017;74: 525−35.
[17] He X, Liu W, Liu Y, et al. Nano artificial periosteum PLGA/MgO/Quercetin accelerates repair of bone defects through promoting osteogenic - angiogenic coupling effect via Wnt/beta-catenin pathway. Mater Today Bio 2022;16: 100348.
[18] Lin Z, Shen D, Zhou W, et al. Regulation of extracellular bioactive cations in bone tissue microenvironment induces favorable osteoimmune conditions to accelerate in situ bone regeneration. Bioact Mater 2021;6:2315−30.
[19] Yuan Z, Wan Z, Wei P, et al. Dual-controlled release of icariin/Mg(2+) from biodegradable microspheres and their synergistic upregulation effect on bone regeneration. Adv Healthcare Mater 2020;9:e2000211.
[20] Leidi M, Dellera F, Mariotti M, Maier JA. High magnesium inhibits human osteoblast differentiation in vitro. Magnes Res 2011;24:1−6.
[21] Yuan Z, Wei P, Huang Y, et al. Injectable PLGA microspheres with tunable magnesium ion release for promoting bone regeneration. Acta Biomater 2019;85:294−309.
[22] Suryavanshi A, Khanna K, Sindhu KR, Bellare J, Srivastava R. Magnesium oxide nanoparticle-loaded polycaprolactone composite electrospun fiber scaffolds for bone-soft tissue engineering applications: in-vitro and in-vivo evaluation. Biomed Mater 2017;12:055011.
[23] Huang S, Liang N, Hu Y, Zhou X, Abidi N. Polydopamine-assisted surface modification for bone biosubstitutes. BioMed Res Int 2016;2016:2389895.
[24] Liu M, Zeng G, Wang K, et al. Recent developments in polydopamine: an emerging soft matter for surface modification and biomedical applications. Nanoscale 2016;8:16819−40.
[25] Ryu JH, Messersmith PB, Lee H. Polydopamine surface chemistry: a decade of discovery. ACS Appl Mater Interfaces 2018;10:7523−40.
[26] Yang Z, Xie L, Zhang B, et al. Preparation of BMP-2/PDA-BCP bioceramic scaffold by DLP 3D printing and its ability for inducing continuous bone formation. Front Bioeng Biotechnol 2022;10:854693.
[27] Liu Y, Ai K, Lu L. Polydopamine and its derivative materials: synthesis and promising applications in energy, environmental, and biomedical fields. Chem Rev 2014;114:5057−115.
[28] Kaushik N, Nhat Nguyen L, Kim JH, Choi EH, Kumar Kaushik N. Strategies for using polydopamine to induce biomineralization of hydroxyapatite on implant materials for bone tissue engineering. Int J Mol Sci 2020;21.
[29] Bhattacharjee P, Kundu B, Naskar D, et al. Silk scaffolds in bone tissue engineering: an overview. Acta Biomater 2017;63:1−17.
[30] Fedorovich NE, Alblas J, Hennink WE, Oner FC, Dhert WJ. Organ printing: the future of bone regeneration? Trends Biotechnol 2011;29:601−6.
[31] He HY, Zhang JY, Mi X, Hu Y, Gu XY. Rapid prototyping for tissue-engineered bone scaffold by 3D printing and biocompatibility study. Int J Clin Exp Med 2015;8:11777−85.
[32] Han C, Li Y, Wang Q, et al. Continuous functionally graded porous titanium scaffolds manufactured by selective laser melting for bone implants. J Mech Behav Biomed Mater 2018;80:119−27.
[33] Staiger MP, Pietak AM, Huadmai J, Dias G. Magnesium and its alloys as orthopedic biomaterials: a review. Biomaterials 2006;27:1728−34.
[34] Yazdimamaghani M, Razavi M, Vashaee D, Moharamzadeh K, Boccaccini AR, Tayebi L. Porous magnesium-based scaffolds for tissue engineering. Mater Sci Eng C 2017;71:1253−66.

[35] Hashemi SS, Rajabi SS, Mahmoudi R, Ghanbari A, Zibara K, Barmak MJ. Poly-urethane/chitosan/hyaluronic acid scaffolds: providing an optimum environment for fibroblast growth. J Wound Care 2020;29:586–96.

[36] Peng W, Ren S, Zhang Y, et al. MgO nanoparticles-incorporated PCL/Gelatin-Derived coaxial electrospinning nanocellulose membranes for periodontal tissue regeneration. Front Bioeng Biotechnol 2021;9:668428.

[37] Liang H, Zhao Y, Yang J, et al. Fabrication, crystalline behavior, mechanical property and in-vivo degradation of poly(l-lactide) (PLLA)-Magnesium oxide whiskers (MgO) nano composites prepared by in-situ polymerization. Polymers 2019;11.

[38] Zhang L, Liu X, Li G, Wang P, Yang Y. Tailoring degradation rates of silk fibroin scaffolds for tissue engineering. J Biomed Mater Res 2019;107:104–13.

[39] van Haaften EE, Duijvelshoff R, Ippel BD, et al. The degradation and performance of electrospun supramolecular vascular scaffolds examined upon in vitro enzymatic exposure. Acta Biomater 2019;92:48–59.

[40] Lai Y, Li Y, Cao H, et al. Osteogenic magnesium incorporated into PLGA/TCP porous scaffold by 3D printing for repairing challenging bone defect. Biomaterials 2019;197:207–19.

[41] Zhao Y, Liang H, Zhang S, Qu S, Jiang Y, Chen M. Effects of magnesium oxide (MgO) shapes on in vitro and in vivo degradation behaviors of PLA/MgO composites in long term. Polymers 2020;12.

[42] Lee GH, Hwang JD, Choi JY, et al. An acidic pH environment increases cell death and pro-inflammatory cytokine release in osteoblasts: the involvement of BAX inhibitor-1. Int J Biochem Cell Biol 2011;43:1305–17.

[43] Ruan C, Hu N, Ma Y, et al. The interfacial pH of acidic degradable polymeric biomaterials and its effects on osteoblast behavior. Sci Rep 2017;7:6794.

[44] Luo Y, Chen S, Shi Y, Ma J. 3D printing of strontium-doped hydroxyapatite based composite scaffolds for repairing critical-sized rabbit calvarial defects. Biomed Mater 2018;13:065004.

[45] Luo Y, Zhai D, Huan Z, et al. Three-dimensional printing of hollow-struts-packed bioceramic scaffolds for bone regeneration. ACS Appl Mater Interfaces 2015;7:24377–83.

[46] Zhang H, Mao X, Zhao D, et al. Three dimensional printed polylactic acid-hydroxyapatite composite scaffolds for prefabricating vascularized tissue engineered bone: an in vivo bioreactor model. Sci Rep 2017;7:15255.

[47] Li W, Zhang S, Liu J, Liu Y, Liang Q. Vitamin K2 stimulates MC3T3-E1 osteoblast differentiation and mineralization through autophagy induction. Mol Med Rep 2019;19:3676–84.

[48] Chen XJ, Shen YS, He MC, et al. Polydatin promotes the osteogenic differentiation of human bone mesenchymal stem cells by activating the BMP2-Wnt/beta-catenin signaling pathway. Biomed Pharmacother 2019;112: 108746.

[49] Zhu Y, Zhao S, Cheng L, et al. Mg(2+) -mediated autophagy-dependent polarization of macrophages mediates the osteogenesis of bone marrow stromal stem cells by interfering with macrophage-derived exosomes containing miR-381. J Orthop Res 2022;40:1563–76.

[50] Zhao X, Han Y, Li J, et al. BMP-2 immobilized PLGA/hydroxyapatite fibrous scaffold via polydopamine stimulates osteoblast growth. Mater Sci Eng C 2017;78:658–66.

[51] Bock N, Pham TL, Nguyen TB, Nguyen TB, Tran HA, Tran PA. Polydopamine coating of uncrosslinked chitosan as an acellular scaffold for full thickness skin grafts. Carbohydr Polym 2020;245:116524.

[52] Meng X, Zhang J, Chen J, et al. KR-12 coating of polyetheretherketone (PEEK) surface via polydopamine improves osteointegration and antibacterial activity in vivo. J Mater Chem B 2020;8:10190–204.

[53] Lee SJ, Lee D, Yoon TR, et al. Surface modification of 3D-printed porous scaffolds via mussel-inspired polydopamine and effective immobilization of rhBMP-2 to promote osteogenic differentiation for bone tissue engineering. Acta Biomater 2016;40:182–91.

[54] Xu M, Zhai D, Xia L, et al. Hierarchical bioceramic scaffolds with 3D-plotted macropores and mussel-inspired surface nanolayers for stimulating osteogenesis. Nanoscale 2016;8:13790–803.

[55] Shim NY, Heo JS. Performance of the polydopamine-graphene oxide composite substrate in the osteogenic differentiation of Mouse embryonic stem cells. Int J Mol Sci 2021;22.

[56] Ma L, Cheng S, Ji X, et al. Immobilizing magnesium ions on 3D printed porous tantalum scaffolds with polydopamine for improved vascularization and osteogenesis. Mater Sci Eng C 2020;117:111303.

[57] Carangelo A, Acquesta A, Monetta T. In-vitro corrosion of AZ31 magnesium alloys by using a polydopamine coating. Bioact Mater 2019;4:71–8.